

The piezoelectric tensor of collagen fibrils determined at the nanoscale

Denise Denning,^{†‡} Jason I. Kilpatrick,[†] Eiichi Fukada,[§] Nan Zhang,^{||} Stefan Habelitz,[⊥] Andrzej Fertala,[¶] Michael D. Gilchrist,^{||} Yuqi Zhang,[#] Syed A. M. Tofail,[#] and Brian J. Rodriguez^{†‡}*

[†] Conway Institute of Biomolecular and Biomedical Research, University College Dublin, Belfield, Dublin 4, Ireland

[‡] School of Physics, University College Dublin, Belfield, Dublin 4, Ireland

[§] Kobayasi Institute of Physical Research, Kokubunji, Tokyo, Japan

^{||} School of Mechanical and Materials Engineering, University College Dublin, Ireland

[⊥] Department of Preventive and Restorative Dental Sciences, University of California, 707 Parnassus Ave., San Francisco, CA 94143-0758, USA

[¶] Department of Orthopaedic Surgery, Thomas Jefferson University, 1015 Walnut Street, Philadelphia, PA 19107, USA

[#] Department of Physics and Bernal Institute, University of Limerick, Ireland

Abstract

Piezoelectric properties of rat tail tendons, sectioned at angles of 0°, 59°, and 90° relative to the plane orthogonal to the major axis, were measured using piezoresponse force microscopy. The piezoelectric tensor at the length scale of an individual fibril was determined from angle-dependent in-plane and out-of-plane piezoelectric measurements. The longitudinal piezoelectric coefficient for individual fibrils at the nanoscale was found to be roughly an order of magnitude greater than that reported for macroscopic measurements of tendon, the low response of which stems from the presence of oppositely oriented fibrils, as confirmed here.

Keywords

Atomic force microscopy, electromechanical coupling, piezoresponse force microscopy, polar orientation, connective tissue, tendon

Corresponding Author

*author to whom correspondence should be addressed: brian.rodriguez@ucd.ie

The use of external electrical stimulation of bone to promote fracture healing dates from 1841 and continues to be used in clinical settings¹⁻³ despite the underlying mechanism remaining elusive. Similarly, mechanical stimulation has been shown to have a pronounced effect on the rate of bone formation.^{4,5} Named after Julius Wolff and widely accepted by clinicians, Wolff's Law describes the response of bone to mechanical loads via mechanotransduction⁶ and implies that bone remodeling can be influenced by both electrical and mechanical stimuli. Electromechanical coupling in bone was first reported by Fukada and Yasuda⁷ who demonstrated that bone behaves as a macroscopic piezoelectric material with a piezoelectric tensor comprising only a d_{14} coefficient ($d_{25}^0 = -d_{14}^0$). Thereafter, the direct piezoelectric effect in bone was linked with the ability of bone to remodel.⁸ Fukada and Yasuda also reported that like bone, tendon, which comprises highly aligned collagen fibrils having a charge dipole corresponding to the amine (N) to carboxyl (C) termini of the constituent collagen molecules, is piezoelectric with a hexagonal C_6 class symmetry,⁹ suggesting that the piezoelectricity of bone is likely due to the presence of collagen. Subsequent studies confirmed that the principal contributor to piezoelectricity in bone is collagen.¹⁰ Recent experiments, where hydroxyapatite (the mineral phase of bone) deposition occurred on cyclically deformed cortical bone collagen (the organic matrix of bone), suggest that piezoelectric generation of electric charge may be a primary mechanism of bone remodeling.¹¹

The complex response of bone to a wide variety of forces (compressive, shear, tensile, etc.) is currently poorly understood. Studies have shown that the microstructure of collagen and Haversian systems are suited to resist these forces.¹² The high degree of structural organization of collagen in bone and the tensorial nature of collagen piezoelectricity imply that the sign and magnitude of piezoelectrically-induced charge will depend on the location within the bone and

the nature of the mechanical load. Thus, collagen piezoelectricity is uniquely suited as a biological cue enabling cells to locally differentiate between mechanical loads of varying magnitude and direction. Large variations in the magnitude of the charge exhibited across the surface of bone have been observed when a stress is applied¹³ – in this regard, piezoelectricity may be a promising explanation for this phenomenon. However, the full piezoelectric tensors of tendon and bone have only been determined on the macroscale and while the crystal structure of collagen is known,¹⁴ the tensor of collagen has only been inferred from macroscale measurements.^{9,15} By their very nature, macroscopic piezoelectric measurements represent an ensemble of nanoscale responses making the identification of piezoelectric coefficients for individual collagen fibrils challenging. Recent nanoscale measurements of a tendon cross section revealed that while collagen fibrils were highly aligned, they were organized into domains of opposite polarity.¹⁶ This fibrillar polar organization may cause the piezoelectric response of adjacent fibrils to cancel out in macroscopic measurements.

Since cellular response to electrical signals occurs at a local scale,¹⁷ determining an accurate piezoelectric tensor for collagen will have significant implications for investigating and exploiting any associated biofunctionality. With the advent of piezoresponse force microscopy (PFM), it is now possible to probe piezoelectricity in biosystems, including collagen,^{18–21} with nanoscale resolution. The longitudinal piezoelectric response of adult humerus and tibia bone under both dry and wet conditions was reported to be nonzero for transverse cuts and zero for longitudinal cuts, perpendicular and parallel to the diaphysial axis, respectively.²² Macroscopically, however, a negligible longitudinal piezoelectric response was reported for transverse cuts of bone,⁷ illustrating a disparity between local and macroscopic measurements. Similarly, limited longitudinal response ($d_{33} = 0.0866$ pm/V) was measured macroscopically in

tendon,^{9,15} yet local measurements again suggest a higher longitudinal signal.¹⁶ Nanoscale shear piezoelectric measurements on collagen, however, were of the same order of magnitude as those seen macroscopically in tendon.¹⁹ These studies highlight the gap in our knowledge between the macro- and nanoscale piezoelectric properties of collagen.

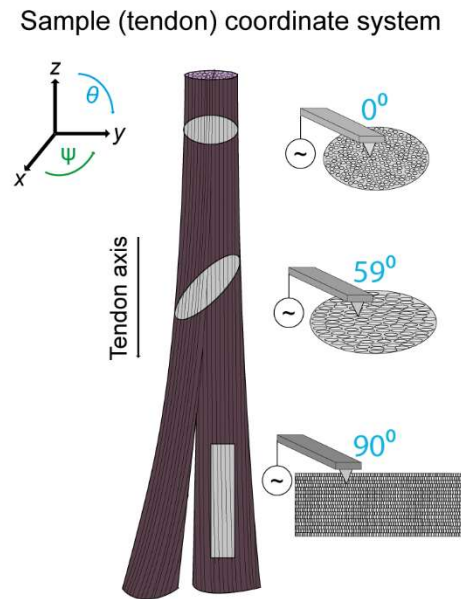


Figure 1. Schematic showing the sample coordinate system and tendon cross sections used in this study.

Here, the piezoelectric tensor of collagen at the individual fibril level is determined using PFM²³ in an attempt to bridge the knowledge gap between the macro- and nanoscale. Due to the hierarchical structure of bone and the mineralization of the collagen contained within, individual collagen fibrils are difficult to isolate. To avoid these difficulties, tendon, which often serves as a model for mineralization studies,²⁴ is used for this study. Both the in-plane (lateral PFM (LPFM)) and out-of-plane (vertical PFM (VPFM)) piezoresponse signals were measured for tendon sectioned at three different angles (0° , 59° and 90°) relative to the plane orthogonal to the

major axis (Figure 1). Measurements were recorded in the laboratory coordinate system and then related to the sample coordinate system in order to calculate piezoelectric coefficients.

Tendon was harvested directly from the tail of a 4 week old rat²⁵ and then fixed in 4% paraformaldehyde for 1 hour prior to embedding in epoxy (Epon 812, Sigma Aldrich). The epoxy resin was cured for 36 hours at 45 °C (lower than the thermal denaturation temperature of rat tail tendon (64 °C)²⁶). Three embedded tendons were trimmed and polished using 280 and 1000 grit silicon carbide grinding paper at 200 – 400 rpm. 10 µm-thick sections were then cut using a microtome (EM UC6, Leica). Two of the cut angles were determined to be 7° and 59° from optical images. The third could not be measured from the optical images and was assumed to be the target angle of 90°. For the piezoelectric tensor analysis, a value of 10° of uncertainty in cut angle was used for error propagation. Standard error propagation techniques were used throughout.²⁷

PFM was performed using an atomic force microscope (AFM) system (MFP-3D, Asylum Research) equipped with an external lock-in amplifier (HF2LI, Zurich Instruments) and a high voltage amplifier (F10A, FLC Electronics). Conductive cantilevers (PPP-EFM, Nanosensors) having a nominal spring constant and resonant frequency of 2.8 N/m and 75 kHz, respectively, were used. Typically, a 30 V ac signal was applied to the tip at 5–7 kHz (LPFM) or 20–25 kHz (VPFM) whilst in contact with the surface (typical imaging force ~ 100 nN). The modulation frequency was chosen to be much lower than the contact resonance to avoid resonant enhancement of the measured signal and to facilitate quantification. The bias-induced surface deformations were demodulated into X and Y Cartesian signals ($X = R \cdot \cos\Phi$ and $Y = R \cdot \sin\Phi$) where R is the amplitude of piezoelectric deformation and Φ is the phase difference between the excitation and the measured signal and contains information on polar ordering, which relates to

the previously described N to C polarity in collagen.¹⁶ PFM images were obtained in contact mode and are presented as the X Cartesian signal. Hence, the images presented contain both the amplitude of piezoelectric deformation and the local polar orientation of the collagen fibrils. In order to determine the characteristic size of regions of uniform polarity, a 2 dimensional (2D) autocorrelation analysis²⁸ was undertaken. 2D autocorrelation analysis was also used to determine the angle, ψ , between the major axis of the cantilever (laboratory x axis) and tendon axis in the x - y plane from the directionality of the PFM phase data (see Table 1).

Table 1 – Experimental parameters for θ and ψ , domain sizes obtained from correlation analysis, and number of locations investigated for each PFM type.

| Nominal θ (°) | Measured θ (°) | θ Error (°) | Minor axis (nm) | Major axis (nm) | Locations | PFM type | ψ (°) |
|----------------------|-----------------------|--------------------|-----------------|------------------|-----------|----------|---|
| 0 | 7 | 10 | 160.8 ± 2.4 | 158.1 ± 2.8 | 4 | VPFM | - |
| | | | | | 5 | VPFM | - |
| 45 | 59 | 10 | 198.3 ± 6.2 | 615.7 ± 24.2 | 4 | LPFM | 85.0 ± 7.0 91.8 ± 10.2 91.6 ± 13.3 95.3 ± 13.3 |
| 90 | 90* | 10 | 162.7 ± 4.4 | 5370 ± 30 | 3 | LPFM | 70.5 ± 6.5 63.5 ± 5.3 71.7 ± 4.1 |

* Assumed angle

For the determination of the piezoelectric tensor, we assume that the $\theta = 0^\circ$ and $\theta = 90^\circ$ cuts are accurate and use the measured value of $\theta = 59^\circ$ for the third cut. We use the measured values of θ and ψ along with their uncertainties for error propagation (Table 1). Single point measurements were conducted to determine the relevant piezoelectric coefficients, whereby the tip was placed in contact with the surface at 4 locations on average per sample with the amplitude (piezoelectric deformation) measured as a function of applied ac voltage. The piezoelectric coefficient (in pm/V) was then determined from the slope of the resulting graph. The vertical inverse optical lever sensitivity (InvOLS) was obtained from the constant

compliance region of contact mode force curves measured on hard surface.²⁹ A geometrical conversion was used to obtain the lateral InvOLS,³⁰ based on geometrical dimensions determined via scanning electron microscopy (SEM) of the cantilevers used in this study and taking into account the gain ratio between the deflection and lateral signals (measured to be 4.0 for the AFM used). The vertical InvOLS for the probes used was typically in the range of 68 – 81 nm/V and the calculated lateral InvOLS was typically in the range of 2.7×10^3 – 3.1×10^3 nm/V. With the same type of AFM and a similar probe, Choi et al.³¹ measured a lateral InvOLS of 8.24×10^3 nm/V on a barium titanate single crystal using a friction loop approach, finding good agreement between their measured piezoelectric coefficient and literature values and lending confidence to our calculated lateral InvOLS value. The difference in lateral InvOLS values obtained may relate to differences in the nature of the geometric calculation versus the friction-based method utilized by Choi et al. Lateral InvOLS calibration remains a challenging topic in PFM³² where not only the beam properties but also the nature of the tip-sample contact³¹ must be taken into consideration. For a comprehensive discussion of lateral InvOLS calibration, see these reviews.^{33–37} Furthermore, it is important to point out that convergence of local PFM and macroscopic piezoelectric measurements is unlikely due to the highly inhomogeneous electric field at the tip and corresponding locally confined deformation, which might be affected by sample-induced clamping. Thus, the measured response is sensitive not only to piezoelectric, but also elastic moduli, and dielectric constants.³⁸

To determine each piezoelectric coefficient for collagen, the relationship between the measured (laboratory) and sample coordinate system must be considered. For a known sample orientation, the laboratory coordinate system (d_{ij}) can be related to the sample coordinate system

(d_{kl}^0) .³⁹ For tendon, with C_6 hexagonal symmetry, $d_{31}^0 = d_{32}^0$, $d_{14}^0 = -d_{25}^0$, and $d_{15}^0 = d_{24}^0$ and the piezoelectric tensor is:

$$d_{ij}^0 = \begin{pmatrix} 0 & 0 & 0 & d_{14}^0 & d_{15}^0 & 0 \\ 0 & 0 & 0 & d_{15}^0 & -d_{14}^0 & 0 \\ d_{31}^0 & d_{31}^0 & d_{33}^0 & 0 & 0 & 0 \end{pmatrix} \quad (1)$$

The hexagonal symmetry simplifies the number of coefficients that must be determined in order to reconstruct the entire piezoelectric tensor at the local scale via a combination of VPFM and LPFM measurements on the three sections of tendon. In PFM, the piezoelectric tensor for collagen in laboratory coordinates⁴⁰ can then be determined using the following equations:

$$d_{33} = \cos \theta (d_{33}^0 \cos^2 \theta + (d_{15}^0 + d_{31}^0) \sin^2 \theta) \quad (2)$$

$$d_{34} = \sin \theta (2(d_{33}^0 - d_{31}^0 - d_{15}^0) \cos^2 \theta \cos \psi - d_{14}^0 \cos \theta \sin \psi + d_{15}^0 \cos \psi) \quad (3)$$

$$d_{35} = \sin \theta (2(d_{33}^0 - d_{31}^0 - d_{15}^0) \cos^2 \theta \sin \psi + d_{14}^0 \cos \theta \cos \psi + d_{15}^0 \sin \psi) \quad (4)$$

where θ is the angle between the major axis of the tendon (sample z axis) and the direction of applied electric field (laboratory z axis), and ψ is the angle between the major axis of the cantilever (laboratory x axis) and tendon axis in the x - y plane.

For the 0° tendon section, the applied electric field is in the same direction as the major axis of the tendon. This is independent of ψ and allows for the direct measurement of the d_{33}^0 piezoelectric coefficient ($d_{33}^0 = d_{33}$ when $\theta = 0^\circ$), thus only VPFM of this section is required. Additionally, when the tendon axis is perpendicular to the applied field and to the major axis of

the cantilever (90° section), the d_{15}^0 piezoelectric coefficient can be directly measured from d_{34} ($d_{15}^0 = d_{34}$ when $\theta = \psi = 90^\circ$), i.e., LPFM of this section.

To determine the remaining piezoelectric coefficients, VPFM and LPFM were measured from a third section of tendon ($\theta = 59^\circ$). For the general case, equation (2) can be solved to obtain:

$$d_{31}^0 = -\csc^2 \theta (d_{15}^0 + (-d_{15}^0 + d_{33}) \cos^2 \theta - d_{33} \sec \theta) \quad (5)$$

Since both d_{33}^0 and d_{15}^0 were directly measured using VPFM and LPFM on the 0° and 90° sections, respectively, it is possible to determine d_{31}^0 from equation (5) and VPFM for this cross section. For the special case, $\theta = 45^\circ$, $d_{31}^0 = 2\sqrt{2}d_{33} - d_{15}^0 - d_{33}^0$ (see Supporting Information).

Similarly, for a shear signal (LPFM) detected from this section ($\theta = 59^\circ$; ψ nominally 90°), equation (3) becomes:

$$d_{14}^0 = \sec \theta [d_{34} \csc \theta \sec \psi + (d_{31}^0 - d_{33}^0 + (d_{15}^0 + d_{31}^0 - d_{33}^0) \cos 2\theta) \tan \psi] \quad (6)$$

Thus, once the d_{33}^0 , d_{15}^0 , and d_{31}^0 coefficients have been determined, it is possible to calculate the d_{14}^0 coefficient and reconstruct the entire piezoelectric tensor of collagen (assuming it has C_6 symmetry, as reported). For the special case, $\theta = 45^\circ$ and $\psi = 90^\circ$, d_{14}^0 can be directly measured as $d_{34} = -\frac{1}{2}d_{14}^0$ (see Supporting Information).

A 3D AFM height image from the 0° section with a mixed VPFM piezoresponse image overlaid, which contains both amplitude and phase information (d_{33} coefficient map), is shown in Figure 2a. Regular circular features are visible throughout the image from the height data, each of which may correspond to individual fibril cross sectioned ends. Bright (yellow) and dark (purple) regions represent domains (i.e., regions of uniform phase response) of opposite polarization. Round features present in the AFM height data were measured via line profiles and found to have an average diameter of 184 ± 39 nm ($n = 15$). In consideration of the slight miscut of 7° , this value is in good agreement with the average diameter of tendon in 4 week old rat (~ 170 nm), as measured by electron microscopy.⁴¹ A gap in the surface is evident on the left of Figure 2a where no domains are visible, perhaps signifying a boundary between fascicles.

A 3D AFM height image of the 90° section (tendon axis is orthogonal to major axis of the cantilever and nominal values $\theta = \psi = 90^\circ$) with the mixed d_{15} coefficient image (LPFM) overlaid is shown in Figure 2b. From the height data, parallel collagen fibrils can be seen, which exhibit the well-known 67 nm D-periodicity associated with type I collagen. The periodicity was measured to be 66 ± 1 nm by subtracting any long-range background topography from a representative line profile and fitting a sine function. A boundary between two fascicles might explain the topographic feature parallel to the fibrils that is present in the image. The LPFM overlay confirms the expected shear piezoelectricity along the collagen fibril axis. An antiparallel polar orientation of fibrils is observed down to the individual fibril level, similar to that seen previously for rat tendon,²¹ fascia,²⁰ and eye tissues.¹⁶

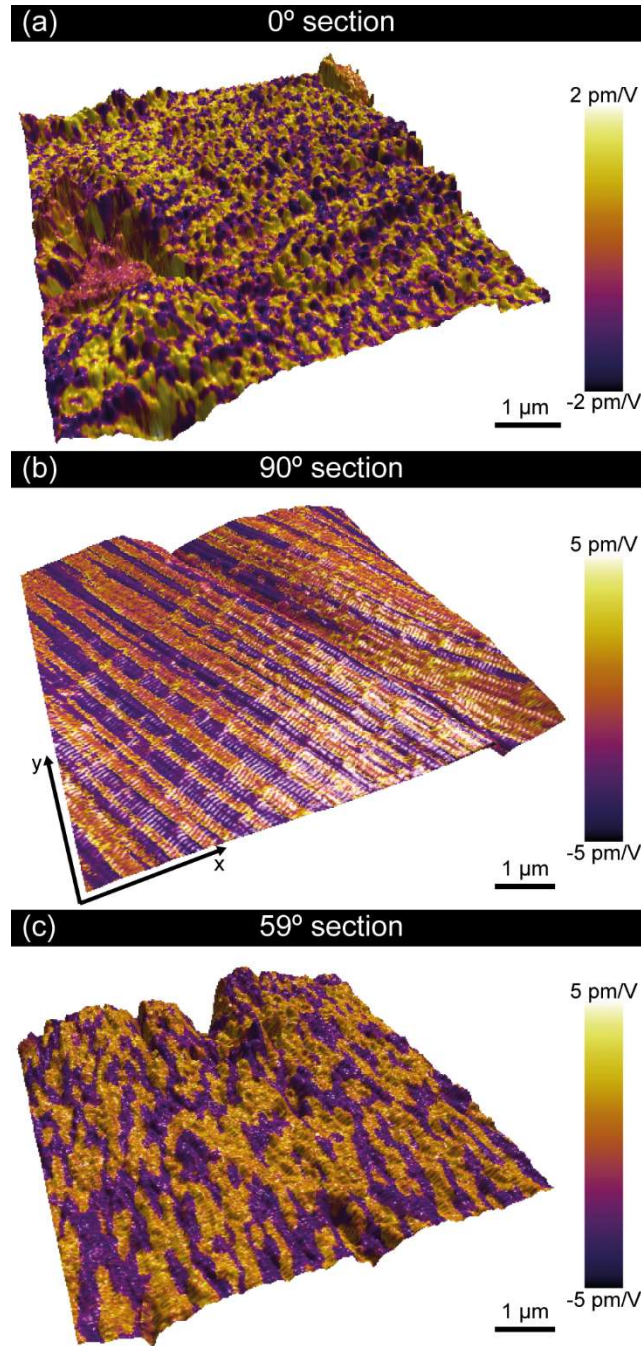


Figure 2. PFM maps of 0°, 59°, and 90° sections of rat tail tendon. (a) Mixed VPFM image ($d_{33} = d_{33}^0$ coefficient map) of 0° section, comprising fibril cross sections. (b) Mixed LPFM image ($d_{34} = d_{15}^0$ coefficient map) of 90° section, comprising fibrils parallel to the surface. (c) Mixed VPFM image (d_{34} piezoresponse map) of intermediate 59° section.

A 3D height image of the 59° section with a d_{34} piezoresponse map (VPFM) overlaid is shown in Figure 2c. By combining measurements of VPFM and LPFM on the 59° section, it is possible to determine both d_{31}^0 and d_{14}^0 coefficients from equations (5) and (6), respectively, and thus reconstruct the collagen piezoelectric tensor at the individual fibril scale. It is important that $\psi = 90^\circ$ when measuring VPFM of this section; any deviation can lead to buckling deflections due to in-plane shear deformations, influencing the determination of d_{31}^0 and d_{14}^0 . As ψ was determined to roughly equal 90° (Table 1), the effect of buckling is minimized.

A 2D autocorrelation function was obtained using the mixed PFM images for each section and the characteristic domain size was calculated in x and y directions. It was determined that the domain size in the x direction (fibril diameter; minor axis in Table 1) for the 0°, 59°, and 90° sections was 160.8 ± 2.4 nm, 198.3 ± 6.2 nm, and 162.7 ± 4.4 nm, respectively. These values are in good agreement under the assumption that each domain is composed of a single collagen fibril. The domain size in the y direction (fibril length; major axis in Table 1) for the 0°, 59°, and 90° sections was 158.1 ± 2.8 nm, 615.7 ± 24.2 nm, and 5.37 ± 0.03 μm , illustrating the elongation of the domain sizes along the axis corresponding to the fibril length with increasing sectioning angle. For the 0° section, the domain is circular, having a diameter similar to those measured from topographical features and reported in the literature.⁴¹ This agreement suggests that the typical piezoelectric domain in the 0° cross section of tendon corresponds to an individual cross sectioned fibril end. However, assuming a fibril diameter of 158.1 nm, the domain size in y for the 59° section is roughly twice the expected value of 307 nm, suggesting that perhaps the average diameter of the fibril or number of fibrils comprising a domain, i.e., having the same polar orientation, along the length of the tendon can vary.

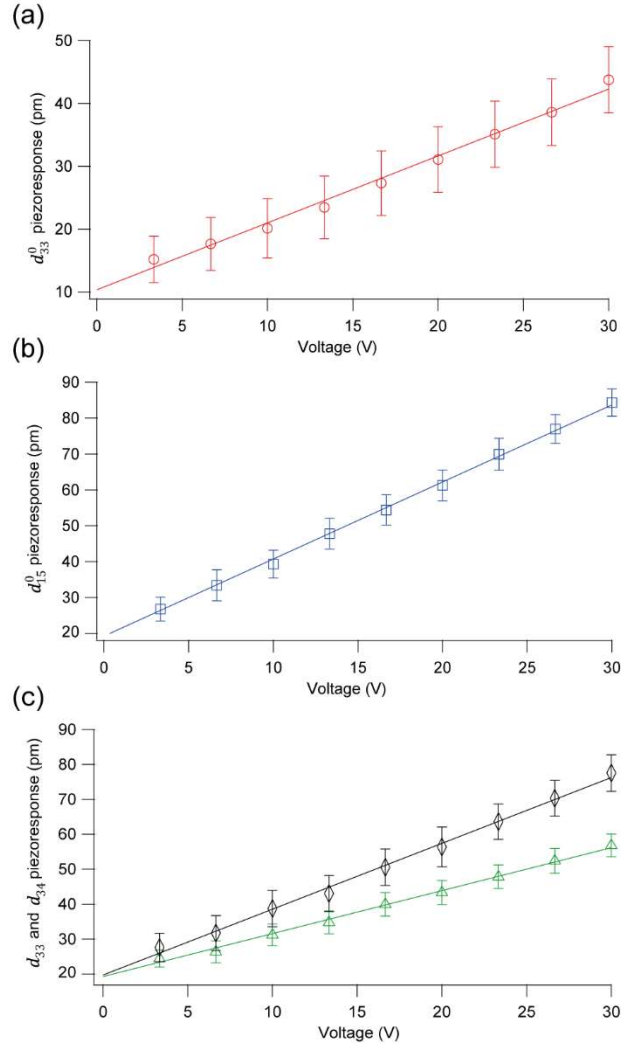


Figure 3. Point measurement graphs displaying piezoelectric responses in the three sections. (a) VPFM response (\circ) measured on 0° section as a function of applied ac voltage ($d_{33} = d_{33}^0$). (b) LPFM response (\square) measured on 90° section as a function of applied ac voltage ($d_{34} = d_{15}^0$). (c) LPFM response (\diamond) and VPFM response (Δ) measured on 59° section as a function of applied voltage, allowing for the deduction of remaining piezoelectric coefficients.

A typical VPFM response as a function of applied ac voltage obtained for the 0° section is shown in Figure 3a. Such nanoscale point measurements are limited by the size of the tip radius and give local values independent of domain size. As described by equation (2) for this case, the slope of this graph yields the d_{33}^0 piezoelectric coefficient. The average slope for all measurements from this cut was 0.89 ± 0.08 pm/V. This value is lower than that reported for

local measurements on transverse cuts of bone²² and might indicate differences in calibration. Figure 3b is a representative LPFM response versus applied ac voltage acquired on the 90° section. In this case, equation (4) simplifies to $d_{34} = d_{15}^0$ and the slope of Figure 3b is a direct measurement of the d_{15}^0 piezoelectric coefficient. The average slope for all measurements from this cut was 6.21 ± 2.93 pm/V. This calibration-dependent value is the same order of magnitude (~ 2.6 pm/V) as determined through simulation⁴² and greater than the experimental values ($\leq \sim 1$) reported elsewhere.^{19,20,43} This discrepancy may be due to the fact that the fibrils in those studies were mounted on a substrate or at the surface of partially demineralized bone and suggests the sample fixation utilized in this work did not significantly alter the electromechanical properties, although that is an avenue of future investigation. Furthermore, there may be a source-dependent variation; Fukada and Yasuda reported that d_{15}^0 for bovine Achilles tendon was ~ 2.6 times that of equine Achilles tendon.⁹ The high uncertainty for d_{15}^0 stems from the uncertainty in lateral calibration and the uncertainty in ψ . Representative d_{33} and d_{34} piezoresponse amplitude signals as a function of applied ac voltage are shown in Figure 3c. Using equations (5) and (6), it was possible to determine both the d_{31}^0 and d_{14}^0 coefficients (-4.84 ± 2.96 pm/V and -12.00 ± 2.60 pm/V, respectively), thus successfully reconstructing the entire piezoelectric tensor for collagen at the individual fibril level for the first time (equation (7)). The high uncertainty for d_{15}^0 dominates the derived uncertainty in d_{31}^0 and d_{14}^0 .

$$d_{ij}^0 = \begin{pmatrix} 0 & 0 & 0 & -12.00 \pm 2.60 & 6.21 \pm 2.93 & 0 \\ 0 & 0 & 0 & 6.21 \pm 2.93 & 12.00 \pm 2.60 & 0 \\ -4.84 \pm 2.96 & -4.84 \pm 2.96 & 0.89 \pm 0.08 & 0 & 0 & 0 \end{pmatrix} \quad (7)$$

These results show an apparent discrepancy between electromechanical measurements recorded at the nanoscale and the macroscale. The tensor previously calculated at the macroscale for tendon^{9,15} ($d_{33}^0 = 0.0866$ pm/V; $d_{31}^0 = 0.066$ pm/V; $d_{14}^0 = -2.66$ pm/V; $d_{15}^0 = 1.4$ pm/V) appears to greatly underestimate most coefficients (notably d_{33}^0 and d_{31}^0) when compared to the nanoscale coefficients reported here ($d_{33}^0 = 0.89$ pm/V; $d_{31}^0 = -4.84$ pm/V; $d_{14}^0 = -12$ pm/V; $d_{15}^0 = 6.21$ pm/V). The average piezoresponse (which includes polar orientation information) of d_{33}^0 images ($n = 10$, typically 8×8 μm) was calculated to be -0.13 ± 0.19 pm/V, highlighting that macroscopic measurements yield lower values due to the averaging of opposing polar orientations. Such observations have been made for polycrystalline piezoelectric films comprising grains of mixed orientations. Histogram analysis of the VPFM phase images of tendon (d_{33}^0) yields an average difference between the number of domains pointing up versus down (comprising opposite N to C polarities of the fibrils) of 17%. Thus, despite measuring local response on the order of ~ 1 pm/V, the measured averaged response at the microscale (as measured via averaging multiple images) is lower, in line with macroscopic measurements and suggesting a similar mechanism. It remains to be seen if the difference between local and macroscopic responses of hierarchically structured bone is biofunctionally significant, e.g., local piezoelectrically-induced charge may be relevant for calcification, and should be the subject of further investigations. The difference between nanoscale and macroscale measurements affects the determination of d_{31}^0 as well. Notably, the coefficient becomes negative, in part because $d_{15}^0 > d_{33}^0$ (equation 5) and can be influenced by buckling deflections due to in-plane shear deformations. Interestingly, the ratio of $|d_{14}^0|:|d_{15}^0|$ is $\sim 1.9:1$ for both tendon and fibril. Further work could explore whether the sign and value of d_{31}^0 depends on the location along the tendon from which the cross section is prepared.

In summary, a general approach has been implemented for determining the piezoelectric tensor of a piezoelectric object of known symmetry and demonstrated on collagen fibrils. The technique can be applied to other biomaterials including collagen fibres^{44,45} for tissue engineering applications and diphenylalanine structures^{46,47} for biosensing applications. The approach can be further refined by (i) more accurately achieving cross sectioning at desired angles that might simplify the piezoelectric coefficient tensor equations and reduce uncertainties, and (ii) establishing a robust procedure for measuring and verifying the sample-dependent³¹ lateral InvOLS, which is an ongoing problem in the quantification of LPFM.³² Recently, Vasilev et al. reported that the full piezoelectric tensor of unipolar diphenylalanine microtubes having hexagonal symmetry could be determined by PFM, highlighting the suitability of the approach.⁴⁸ The results reported here on tendon are particularly relevant for piezoelectric measurements performed at the macroscopic scale where a sample contains domains of oppositely oriented polarizations. In these cases, piezoelectric coefficient values can be greatly underestimated or even negated. The piezoelectric tensor of collagen at the individual fibril level determined in this study will be important for future investigations of biofunctionality of piezoelectricity in collagenous materials, as the cellular responses to stress and electrical stimuli occur, and are sensed, at the local scale. Importantly, the d_{33}^0 of an individual collagen fibril is ~ 10 times greater than previously reported for tendon macroscopically, suggesting applications based on longitudinal, in addition to shear piezoelectricity, are viable, including biomaterials-based energy harvesting applications.^{49–51}

Author Contributions

The manuscript was written through contributions of all authors. All authors have given approval to the final version of the manuscript.

Acknowledgement

This publication has emanated from research conducted with the financial support of Science Foundation Ireland under grant numbers SFI10/RFP/MTR2855 and SFI12/IA/1449 and was further facilitated by SFI13/CW/B2538, SFI07/IN1/B931, and UCD Research (SF891). The authors also acknowledge the support of NANOREMEDIES, which is funded by the Programme for Research in Third Level Institutions, Cycle 5 and co-funded by the European Regional Development Fund. Part of this work was supported by the European Union's Horizon 2020 research and innovation program under the Marie Skłodowska-Curie grant agreement number 644175. The authors gratefully acknowledge the group of Dr. J. O'Connor, UCD for donating the rat tails for this study, Dr. B. Lukasz, UCD for assistance with SEM imaging, and the UCD Conway Imaging Core.

References

- (1) Hartshorne, E. On the causes and treatment of pseudarthrosis, and especially of that form of it sometimes called supernumerary joint. *Am J Med Sci* **1841**, *1*, 121–156.
- (2) Yasuda, I. The classic: Fundamental aspects of fracture treatment by Iwao Yasuda, reprinted from J. Kyoto Med. Soc., 4:395-406, 1953. *Clin. Orthop. Relat. Res.* **1977**, No. 124, 5–8.
- (3) Assiotis, A.; Sachinis, N. P.; Chalidis, B. E. Pulsed electromagnetic fields for the treatment of tibial delayed unions and nonunions. A prospective clinical study and review of the literature. *J. Orthop. Surg. Res.* **2012**, *7* (1), 24 DOI: 10.1186/1749-799X-7-24.
- (4) Chambers, T. J.; Evans, M.; Gardner, T. N.; Turner-Smith, A.; Chow, J. W. M. Induction of bone formation in rat tail vertebrae by mechanical loading. *Bone Miner.* **1993**, *20* (2), 167–178 DOI: 10.1016/S0169-6009(08)80025-6.
- (5) Turner, C. H. Three rules for bone adaptation to mechanical stimuli. *Bone* **1998**, *23* (5), 399–407 DOI: 10.1016/S8756-3282(98)00118-5.
- (6) Bertram, J. E. A.; Swartz, S. M. The ‘Law of Bone Transformation: A Case of Crying Wolff? *Biol. Rev.* **1991**, *66* (3), 245–273 DOI: 10.1111/j.1469-185X.1991.tb01142.x.
- (7) Fukada, E.; Yasuda, I. On the piezoelectric effect of bone. *J. Phys. Soc. Japan* **1957**, *12* (10), 1158–1162 DOI: 10.1143/JPSJ.12.1158.
- (8) Fukada, E. History and recent progress in piezoelectric polymers. *IEEE Trans. Ultrason. Ferroelectr. Freq. Control* **2000**, *47* (6), 1277–1290 DOI: 10.1109/58.883516.
- (9) Fukada, E.; Yasuda, I. Piezoelectric Effects in Collagen. *Jpn. J. Appl. Phys.* **1964**, *3* (2), 117–121 DOI: 10.1143/JJAP.3.117.
- (10) Marino, A. A.; Becker, R. O.; Soderholm, S. C. Origin of the piezoelectric effect in bone. *Calcif. Tissue Res.* **1971**, *8* (1), 177–180 DOI: 10.1007/BF02010135.
- (11) Noris-Suárez, K.; Lira-Olivares, J.; Ferreira, A. M.; Feijoo, J. L.; Suárez, N.; Hernández, M. C.; Barrios, E. In Vitro Deposition of Hydroxyapatite on Cortical Bone Collagen Stimulated by Deformation-Induced Piezoelectricity. *Biomacromolecules* **2007**, *8* (3), 941–948 DOI: 10.1021/bm060828z.
- (12) Bromage, T. G.; Goldman, H. M.; McFarlin, S. C.; Warshaw, J.; Boyde, A.; Riggs, C. M. Circularly polarized light standards for investigations of collagen fiber orientation in bone. *Anat. Rec.* **2003**, *274B* (1), 157–168 DOI: 10.1002/ar.b.10031.
- (13) McElhaney, J. H. The charge distribution on the human femur due to load. *J. Bone Joint Surg. Am.* **1967**, *49* (8), 1561–1571.
- (14) Ramachandran, G. N.; Kartha, G. Structure of Collagen. *Nature* **1954**, *174* (4423), 269–270 DOI: 10.1038/174269c0.

- (15) Gundjian, A. A.; Chen, H. L. Standardization and interpretation of the electromechanical properties of bone. *IEEE Trans. Biomed. Eng.* **1974**, *21* (3), 177–182 DOI: 10.1109/TBME.1974.324380.
- (16) Denning, D.; Alilat, S.; Habelitz, S.; Fertala, A.; Rodriguez, B. J. Visualizing molecular polar order in tissues via electromechanical coupling. *J. Struct. Biol.* **2012**, *180* (3), 409–419 DOI: 10.1016/j.jsb.2012.09.003.
- (17) Ingber, D. E. Cellular mechanotransduction: putting all the pieces together again. *FASEB J.* **2006**, *20* (7), 811–827 DOI: 10.1096/fj.05-5424rev.
- (18) Kalinin, S. V.; Rodriguez, B. J.; Jesse, S.; Thundat, T.; Gruverman, A. Electromechanical imaging of biological systems with sub-10 nm resolution. *Appl. Phys. Lett.* **2005**, *87* (5) DOI: 10.1063/1.2006984.
- (19) Minary-Jolandan, M.; Yu, M.-F. Nanoscale characterization of isolated individual type I collagen fibrils: polarization and piezoelectricity. *Nanotechnology* **2009**, *20* (8), 085706 DOI: 10.1088/0957-4484/20/8/085706.
- (20) Harnagea, C.; Vallières, M.; Pfeffer, C. P.; Wu, D.; Olsen, B. R.; Pignolet, A.; Légaré, F.; Gruverman, A. Two-dimensional nanoscale structural and functional imaging in individual collagen type I fibrils. *Biophys. J.* **2010**, *98* (12), 3070–3077 DOI: 10.1016/j.bpj.2010.02.047.
- (21) Denning, D.; Abu-Rub, M. T.; Zeugolis, D. I.; Habelitz, S.; Pandit, A.; Fertala, A.; Rodriguez, B. J. Electromechanical properties of dried tendon and isoelectrically focused collagen hydrogels. *Acta Biomater.* **2012**, *8* (8), 3073–3079 DOI: 10.1016/j.actbio.2012.04.017.
- (22) Halperin, C.; Mutchnik, S.; Agronin, A.; Molotskii, M.; Urenski, P.; Salai, M.; Rosenman, G. Piezoelectric effect in human bones studied in nanometer scale. *Nano Lett.* **2004**, *4* (7), 1253–1256 DOI: 10.1021/nl049453i.
- (23) Denning, D.; Guyonnet, J.; Rodriguez, B. J. Applications of piezoresponse force microscopy in materials research: from inorganic ferroelectrics to biopiezoelectrics and beyond. *Int. Mater. Rev.* **2016**, *61* (1), 46–70 DOI: 10.1179/1743280415Y.0000000013.
- (24) Landis, W.; Song, M.; Leith, A.; McEwen, L.; McEwen, B. Mineral and Organic Matrix Interaction in Normally Calcifying Tendon Visualized in Three Dimension by High-Voltage Electron Microscopic Tomography and Graphic Image Reconstruction. *J. Struct. Biol.* **1993**, 39–54 DOI: 10.1006/jsbi.1993.1003.
- (25) Rajan, N.; Habermehl, J.; Coté, M.-F.; Doillon, C. J.; Mantovani, D. Preparation of ready-to-use, storable and reconstituted type I collagen from rat tail tendon for tissue engineering applications. *Nat. Protoc.* **2006**, *1* (6), 2753–2758 DOI: 10.1038/nprot.2006.430.
- (26) Miles, C. A.; Avery, N. C.; Rodin, V. V.; Bailey, A. J. The increase in denaturation temperature following cross-linking of collagen is caused by dehydration of the fibres. *J. Mol. Biol.* **2005**, *346* (2), 551–556 DOI: 10.1016/j.jmb.2004.12.001.

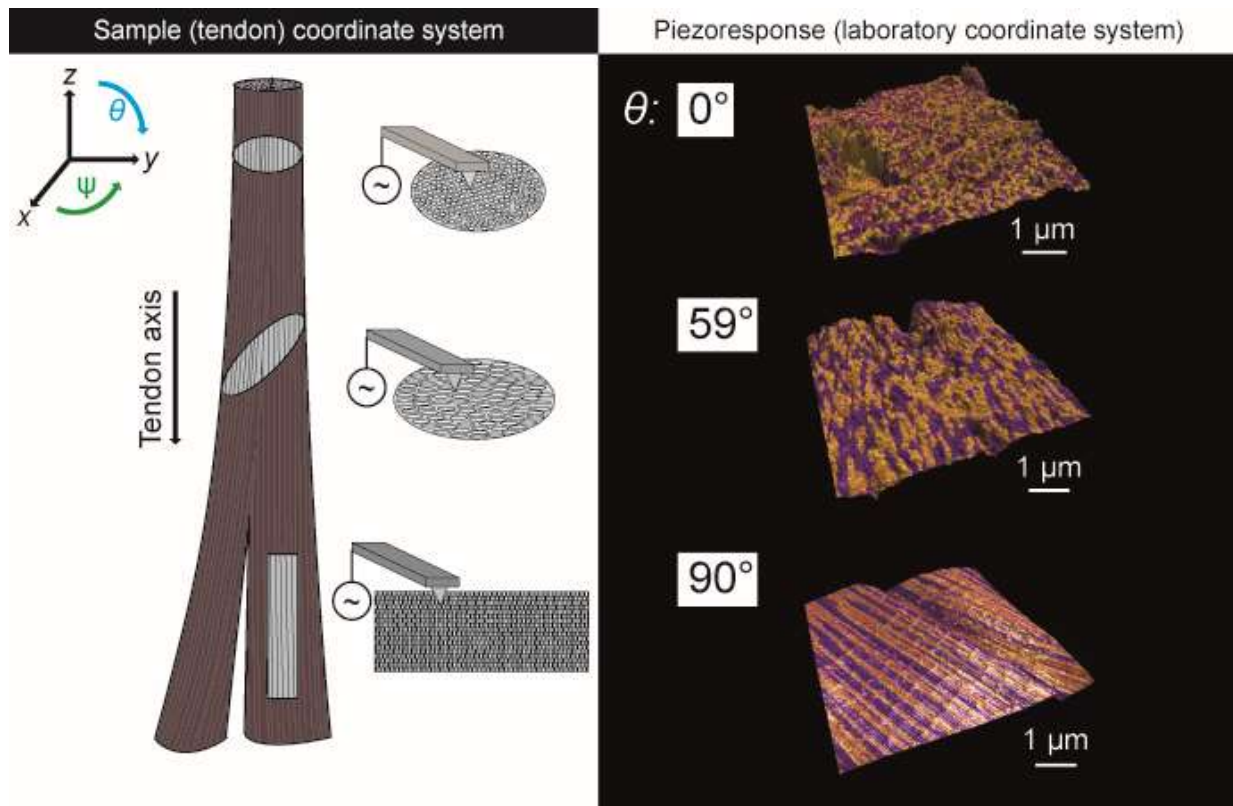
- (27) Ku, H. H. Notes on the use of propagation of error formulas. *J. Res. Natl. Bur. Stand. Sect. C Eng. Instrum.* **1966**, 70C (4), 263 DOI: 10.6028/jres.070C.025.
- (28) Shvartsman, V. V.; Kholkin, A. L. Evolution of nanodomains in 0.9PbMg_{1/3}Nb_{2/3}O₃-0.1PbTiO₃ single crystals. *J. Appl. Phys.* **2007**, 101 (6), 064108–1 – 5 DOI: 10.1063/1.2713084.
- (29) D'Costa, N. P.; Hoh, J. H. Calibration of optical lever sensitivity for atomic force microscopy. *Rev. Sci. Instrum.* **1995**, 66 (10), 5096 DOI: 10.1063/1.1146135.
- (30) Peter, F.; Rüdiger, A.; Szot, K.; Waser, R.; Reichenberg, B. Sample-tip interaction of piezoresponse force microscopy in ferroelectric nanostructures. *IEEE Trans. Ultrason. Ferroelectr. Freq. Control* **2006**, 53 (12), 2253–2260.
- (31) Choi, H.; Hong, S.; No, K. Quantitative measurement of in-plane cantilever torsion for calibrating lateral piezoresponse force microscopy. *Rev. Sci. Instrum.* **2011**, 82 (11) DOI: 10.1063/1.3660806.
- (32) Denning, D.; Guyonnet, J.; Rodriguez, B. J. Applications of piezoresponse force microscopy in materials research: from inorganic ferroelectrics to biopiezoelectrics and beyond. *Int. Mater. Rev.* **2016**, 61 (1), 46–70 DOI: 10.1179/1743280415Y.0000000013.
- (33) Munz, M. Force calibration in lateral force microscopy: a review of the experimental methods. *J. Phys. D. Appl. Phys.* **2010**, 43 (6), 063001 DOI: 10.1088/0022-3727/43/6/063001.
- (34) Barkley, S. S.; Deng, Z.; Gates, R. S.; Reitsma, M. G.; Cannara, R. J. Quantitative comparison of two independent lateral force calibration techniques for the atomic force microscope. *Rev. Sci. Instrum.* **2012**, 83 (2), 023707 DOI: 10.1063/1.3685243.
- (35) Cain, R. G.; Reitsma, M. G.; Biggs, S.; Page, N. W. Quantitative comparison of three calibration techniques for the lateral force microscope. *Rev. Sci. Instrum.* **2001**, 72 (8), 3304 DOI: 10.1063/1.1386631.
- (36) Pettersson, T.; Nordgren, N.; Rutland, M. W.; Feiler, A. Comparison of different methods to calibrate torsional spring constant and photodetector for atomic force microscopy friction measurements in air and liquid. *Rev. Sci. Instrum.* **2007**, 78 (9), 093702 DOI: 10.1063/1.2779215.
- (37) Palacio, M. L. B.; Bhushan, B. Normal and Lateral Force Calibration Techniques for AFM Cantilevers. *Crit. Rev. Solid State Mater. Sci.* **2010**, 35 (2), 73–104 DOI: 10.1080/10408430903546691.
- (38) Pan, K.; Liu, Y. Y.; Liu, Y. M.; Li, J. Y. Analyzing piezoresponse force microscopy for reconstruction of probed ferroelectric structures. *J. Appl. Phys.* **2012**, 112 (5) DOI: 10.1063/1.4746034.
- (39) Cady, W. G. *Piezoelectricity*; McGraw-Hill: New York, NY, 1947.
- (40) Sharma, P.; Wu, D.; Poddar, S.; Reece, T. J.; Ducharme, S.; Gruverman, A. Orientational

- imaging in polar polymers by piezoresponse force microscopy. *J. Appl. Phys.* **2011**, *110* (5), 052010 DOI: 10.1063/1.3623765.
- (41) Scott, J. E.; Orford, C. R.; Hughes, E. W. Proteoglycan-collagen arrangements in developing rat tail tendon. **1981**, 573–581.
- (42) Zhou, Z.; Qian, D.; Minary-Jolandan, M. Molecular Mechanism of Polarization and Piezoelectric Effect in Super-Twisted Collagen. *ACS Biomater. Sci. Eng.* **2016**, acsbiomaterials.6b00021 DOI: 10.1021/acsbiomaterials.6b00021.
- (43) Minary-Jolandan, M.; Yu, M.-F. Uncovering nanoscale electromechanical heterogeneity in the subfibrillar structure of collagen fibrils responsible for the piezoelectricity of bone. *ACS Nano* **2009**, *3* (7), 1859–1863 DOI: 10.1021/nn900472n.
- (44) Zeugolis, D. I.; Paul, G. R.; Attenburrow, G. Cross-linking of extruded collagen fibers-A biomimetic three-dimensional scaffold for tissue engineering applications. *J. Biomed. Mater. Res. Part A* **2009**, *89A* (4), 895–908 DOI: 10.1002/jbm.a.32031.
- (45) Abu-Rub, M. T.; Billiar, K. L.; van Es, M. H.; Knight, A.; Rodriguez, B. J.; Zeugolis, D. I.; McMahon, S.; Windebank, A. J.; Pandit, A. Nano-textured self-assembled aligned collagen hydrogels promote directional neurite guidance and overcome inhibition by myelin associated glycoprotein. *Soft Matter* **2011**, *7*, 2770 DOI: 10.1039/c0sm01062f.
- (46) Kholkin, A.; Amdursky, N.; Bdikin, I.; Gazit, E.; Rosenman, G. Strong Piezoelectricity in Bioinspired Peptide Nanotubes. *ACS Nano* **2010**, *4* (2), 610–614 DOI: 10.1021/nn901327v.
- (47) Ryan, K.; Beirne, J. G.; Redmond, G.; Kilpatrick, J. I.; Guyonnet, J.; Buchete, N.-V.; Kholkin, A. L.; Rodriguez, B. J. Nanoscale piezoelectric properties of self-assembled Fmoc-FF peptide fibrous networks. *ACS Appl. Mater. Interfaces* **2015**, 150521050853004 DOI: 10.1021/acsami.5b01251.
- (48) Vasilev, S.; Zelenovskiy, P.; Vasileva, D.; Nuraeva, A.; Shur, V. Y.; Kholkin, A. L. Piezoelectric properties of diphenylalanine microtubes prepared from the solution. *J. Phys. Chem. Solids* **2016**, *93*, 68–72 DOI: 10.1016/j.jpcs.2016.02.002.
- (49) Ghosh, S. K.; Mandal, D. High-performance bio-piezoelectric nanogenerator made with fish scale. *Appl. Phys. Lett.* **2016**, *109* (10), 103701 DOI: 10.1063/1.4961623.
- (50) Nguyen, V.; Zhu, R.; Jenkins, K.; Yang, R.; Fukada, E.; Yasuda, I.; Halperin, C.; Ghosh, S.; Fukada, E.; Lee, B. Y.; et al. Self-assembly of diphenylalanine peptide with controlled polarization for power generation. *Nat. Commun.* **2016**, *7*, 13566 DOI: 10.1038/ncomms13566.
- (51) Lee, B. Y.; Zhang, J.; Zueger, C.; Chung, W.-J.; Yoo, S. Y.; Wang, E.; Meyer, J.; Ramesh, R.; Lee, S.-W. Virus-based piezoelectric energy generation. *Nat. Nanotechnol.* **2012**, *7* (6), 351–356 DOI: 10.1038/nnano.2012.69.

Table of Contents Figure

The piezoelectric tensor of collagen fibrils determined at the nanoscale

Denise Denning, Jason I. Kilpatrick, Eiichi Fukada, Nan Zhang, Stefan Habelitz, Andrzej Fertala, Michael D. Gilchrist, Yuqi Zhang, Syed A. M. Tofail, and Brian J. Rodriguez



Supporting Information

The piezoelectric tensor of collagen fibrils determined at the nanoscale

Denise Denning, Jason I. Kilpatrick, Eiichi Fukada, Nan Zhang, Stefan Habelitz, Andrzej Fertala, Michael D. Gilchrist, Yuqi Zhang, Syed A. M. Tofail, and Brian J. Rodriguez

2 pages

Equations (2) – (4) can also be written as:

$$d_{33} = 0.5 \cos \theta \left(d_{15}^0 + d_{31}^0 + d_{33}^0 - (d_{15}^0 + d_{31}^0 - d_{33}^0) \right) \cos 2\theta \quad (\text{S1})$$

$$d_{34} = \sin \theta \left(-(d_{31}^0 - d_{33}^0 + (d_{15}^0 + d_{31}^0 - d_{33}^0) \cos 2\theta \cos \psi) - d_{14}^0 \cos \theta \sin \psi \right) \quad (\text{S2})$$

$$d_{35} = \sin \theta \left(d_{14}^0 \cos \theta \cos \psi - (d_{31}^0 - d_{33}^0 + (d_{15}^0 + d_{31}^0 - d_{33}^0) \cos 2\theta) \sin \psi \right) \quad (\text{S3})$$

Equations (2) – (4) can be solved for the piezoelectric tensor coefficients:

$$d_{33}^0 = d_{15}^0 + d_{31}^0 - (d_{15}^0 + d_{31}^0) \sec^2 \theta + d_{33} \sec^3 \theta \quad (\text{S4})$$

$$d_{15}^0 = [2(-d_{31}^0 + d_{33}^0) \cos^2 \theta + d_{14}^0 \cos \theta \cot \psi - d_{34} \csc \theta \csc \psi] \sec 2\theta \quad (\text{S5})$$

$$d_{31}^0 = -\csc^2 \theta (d_{15}^0 + (-d_{15}^0 + d_{33}) \cos^2 \theta - d_{33} \sec \theta) \quad (\text{S6})$$

$$d_{14}^0 = \sec \theta [d_{34} \csc \theta \sec \psi + (d_{31}^0 - d_{33}^0 + (d_{15}^0 + d_{31}^0 - d_{33}^0) \cos 2\theta) \tan \psi] \quad (\text{S7})$$

When the cross sections are cut to the specified angles 0° , 45° , and 90° , the piezoelectric tensor coefficient equations simplify as follows:

For $\theta = 0^\circ$, equation (2) becomes:

$$d_{33} = d_{33}^0 \quad (\text{S8})$$

For $\theta = \psi = 90^\circ$, equation (3) becomes:

$$d_{34} = d_{15}^0 \quad (\text{S9})$$

For $\theta = 45^\circ$ (and $\psi = 90^\circ$ to minimize cantilever buckling), equation (2) becomes:

$$d_{33} = \frac{\sqrt{2}}{4}(d_{15}^0 + d_{31}^0 + d_{33}^0) \quad (\text{S10})$$

Solving for d_{31}^0 :

$$d_{31}^0 = 2\sqrt{2}d_{33} - d_{15}^0 - d_{33}^0 \quad (\text{S11})$$

For $\theta = 45^\circ$ and $\psi = 90^\circ$, equation (3) becomes:

$$d_{34} = -\frac{1}{2}d_{14}^0 \quad (\text{S12})$$

Solving for d_{14}^0 :

$$d_{14}^0 = -2d_{34} \quad (\text{S13})$$

Therefore, it is possible to directly measure d_{14}^0 , d_{15}^0 , and d_{33}^0 . d_{31}^0 can be determined from VPFM measured from the $\theta = 45^\circ$ cut when d_{15}^0 and d_{33}^0 are known.